Quasinormal modes of the Einstein-Maxwell-aether black hole

Wei Xiong,[§] Peng Liu,[†] Cheng-Yong Zhang,[‡] and Chao Niu[*]
Department of Physics and Siyuan Laboratory, Jinan University, Guangzhou 510632, China

(Received 11 February 2022; accepted 12 September 2022; published 30 September 2022)

We study the quasinormal modes of the charged scalar perturbations in the background of the Einstein-Maxwell-aether black hole through three methods (WKB method, continued fraction method, generalized eigenvalue method). Then we propose the specific treatment for the generalized effective potential with ω-dependence and the complete procedure of transforming calculation continued fraction method into finding the zero point of the corresponding complex function numerically. These methods are valid because the results from different methods are consistent. We also investigate the allowed region of the second kind aether black hole among the system parameters (c_{13}, c_{14}, Q). Finally we show the existence of quasiresonances of massive perturbation for Einstein-Maxwell-aether black hole even with large aether parameter.

DOI: 10.1103/PhysRevD.106.064057

I. INTRODUCTION

Quasinormal modes are the eigenvalues of dissipative systems arising by the perturbations of additional fields or metric under the background of black hole [1–4]. The energy dissipation of this system comes from the purely outgoing boundary condition (ingoing waves at horizon and outgoing waves at spatial infinity). The associated linear differential equation, called perturbed equation, generates the non-Hermitian eigenvalue problem because of the non-time symmetry evolution. In astrophysics, quasinormal modes describe the ringdown phase of black hole mergers and allow new tests of general relativity [1]. For theoretical interest, these modes were used to probe various properties of black holes with respect to quantum gravity and investigate the strongly coupled quantum field theories due to the gauge-gravity duality [1,5]. Currently there are gravitational wave (GW) signals detected by LIGO [6,7]. However, various modified gravity theories are not excluded by the current observed data in the gravitational and electromagnetic spectra because of the large uncertainty of the determination of the mass and angular momentum of black holes [8].

The modified gravity theory we are interested in is the Einstein-Maxwell-aether theory, which belongs to the Lorentz violation (LV) models. The reason for introducing Lorentz violation is that Lorentz invariance may not be an exact symmetry at all energies [9]. Different quantum gravity theories have investigated the possibility of the existence of Lorentz violation and the noncommutative field theory, one of the high energy models of spacetime structure, even contains Lorentz violation explicitly [10]. In Einstein-Maxwell-aether theory, the Lorentz violating terms are added to the gravity sector in the dynamical framework [1]. This model assumes that each point of spacetime introduces a preferred timelike direction, marked by an aether vector field u^a. This assumption caused the Lorentz symmetry to be broken down to a rotation subgroup. Many interesting phenomena have been found in this theory [11–16], e.g., a superluminal group velocity is allowed for the modified scalar field [14]. The corresponding light-cones therefore can be completely flat and the causality is not violated by the superluminal phenomena. On the other hand, there are black hole solutions in aether theory [15]. A three-dimensional spacelike hypersurface, called universal horizon, replaces the killing horizon as the event horizon because of the existence of superluminal particle, i.e., because only the universal horizon can trap arbitrarily fast excitations [17]. Furthermore, the Einstein-Maxwell-aether theory here introduces the extra source-Free Maxwell field than pure aether theory. For black holes, the interaction between photon and deformed aether may induce new dynamo-optical effects [15]. The quasinormal modes of the uncharged aether theory have been investigated by Konoplya [18], Ding [19,20] and Churilova [8] for scalar or gravitational perturbations. Churilova [8] argued that the perturbation of the energy-momentum tensor of the aether field should be taken into account for the calculation of the Einstein-aether gravitational perturbations.

In this paper, we first calculate the quasinormal frequencies of the charged massless scalar perturbation in the background of the Einstein-Maxwell-aether black hole. For

[*]Corresponding author.
niuchaophy@gmail.com
[†]phylp@email.jnu.edu.cn
[‡]zhangcy@email.jnu.edu.cn
[§]phyxw@stu2019.jnu.edu.cn

 © 2022 American Physical Society

this charged background, the charged scalar field is naturally introduced to couple with the electromagnetic field [5,21], which can better reveal the new effect of the electromagnetic field on the background of the aether black hole. This perturbation field is necessary for studying the perturbations of charged particles in scalar electrodynamics in the curved charged background [3], which is the Einstein-Maxwell-aether black hole in our cases.

We also confirm the existence of the quasiresonances under the charged aether black hole background, by calculating the massive charged perturbations under these backgrounds. The quasiresonance is the arbitrary long-living mode with real frequency, which is due to the nonzero value of at least one of the boundaries of the effective potential [8,21–32].

The paper is organized as follows. In Sec. II, we introduce the Einstein-Maxwell-aether theory and two black hole solutions. In Sec. III, we specify three different methods for the calculations. The results of the quasinormal frequencies are presented in Sec. IV and the discussion of quasiresonances is shown in Sec. V. We conclude in Sec. VI.

II. EINSTEIN-MAXWELL-AETHER BLACK HOLE

In this section we briefly review the Einstein-Maxwell-aether theory and investigate the scalar perturbation around black hole solutions.

A. Einstein-Maxwell-aether theory

The action of Einstein-Maxwell-aether theory is [15]

$$S=\int d^4x\sqrt{-g}\left[\frac{1}{16\pi G_{æ}}(\mathcal{R}+\mathcal{L}_{æ})+\mathcal{L}_M\right], \tag{1}$$

where the g is the determinant of the metric $g_{\mu\nu}$ and R the Ricci scalar. The constant $G_{æ}$ denotes the Newton's gravitational constants G_N by $G_{æ}=(1-c_{14}/2)G_N$, which is obtained by the renormalization of the total energy of Einstein-aether theory [33]. The aether Lagrangian is

$$\begin{aligned}&\mathcal{L}_{æ}=-Z^{ab}{}_{cd}(\nabla_a u^c)(\nabla_b u^d)+\lambda(u^2+1),\\ &Z^{ab}{}_{cd}=c_1 g^{ab}g_{cd}+c_2\delta^a{}_c\delta^b{}_d+c_3\delta^a{}_d\delta^b{}_d-c_4u^au^bg_{cd},\end{aligned} \tag{2}$$

where c_i $(i=1,2,3,4)$ are coupling constants of the theory and the $\lambda(u^2+1)$ term constraints the vector field to satisfy the normalization condition $u^2=-1$. The source-free Maxwell Lagrangian is

$$\begin{aligned}&\mathcal{L}_M=-\frac{1}{16\pi G_{æ}}\mathcal{F}_{ab}\mathcal{F}^{ab},\\ &\mathcal{F}_{ab}=\nabla_a\mathcal{A}_b-\nabla_b\mathcal{A}_a.\end{aligned} \tag{3}$$

The observational and theoretical bounds of the coupling constants c_i have been investigated by requiring the absence of gravitational Cherenkov radiation for theoretical constants [14,34–36]. Because of the theoretical interest of this LV gravity theory, we impose the following constraints [37],

$$0\le c_{14}<2,\qquad 2+c_{13}+3c_2>0,\qquad 0\le c_{13}<1, \tag{4}$$

where $c_{ij}\equiv c_i+c_j$.

B. Black hole solutions

In asymptotical flat spherically symmetric spacetime, the static metric for Einstein-Maxwell-aether black hole is given by

$$ds^2=-f(r)dt^2+\frac{dr^2}{f(r)}+r^2(d\theta^2+\sin^2\theta d\varphi^2). \tag{5}$$

There are two kinds of exact solutions for the cases $c_{14}=0$, $c_{123}\neq 0$ and $c_{123}=0$, $c_{14}\neq 0$ [15]. They represent two different behaviors of propagation speed of spin-0 mode with respect to linearized aether-metric perturbations around flat spacetime respectively [17,38]. In the first kind aether black hole ($c_{14}=0$, $c_{123}\neq 0$), the metric function is

$$\begin{aligned}&f(r)=1-\frac{r_0}{r}+\frac{Q^2}{r^2}+\frac{c_{13}B}{(1-c_{13})r^4},\\ &B=\frac{(r_0-\sqrt{-32Q^2+9r_0^2})(3r_0+\sqrt{-32Q^2+9r_0^2})^3}{4096},\end{aligned} \tag{6}$$

where ADM mass is given by $r_0/2G_{æ}$, with the constraint of charged $Q\le r_0/2$ which is obtained by requiring regularity of the aether theory for each point in the spacetime [15]. This constraint is the same as that given in the Reissner-Nordström black hole. The metric function shows that the aether correction term is added as $\mathcal{O}(1/r^4)$ in the metric and this correction term vanishes when $c_{13}\to 0$.

The metric function of the second kind aether black hole ($c_{123}=0$, $c_{14}\neq 0$) is given by

$$\begin{aligned}&f(r)=1-\frac{r_0}{r}-\frac{r_u(r_0+r_u)}{r^2},\\ &r_u=\frac{r_0}{2}\left(\sqrt{\frac{2-c_{14}}{2(1-c_{13})}-\frac{4Q^2}{(1-c_{13})r_0^2}}-1\right),\end{aligned} \tag{7}$$

with the following constraints

$$\begin{aligned}&Q\le\frac{r_0}{2}\sqrt{c_{13}-\frac{c_{14}}{2}},\\ &c_{13}\ge\frac{c_{14}}{2}.\end{aligned} \tag{8}$$

C. Massless charged scalar perturbation

Here, we present a massless charged scalar perturbation around black hole solutions (5). For massless charged scalar perturbation, the first-order perturbation $\mathcal{O}(\epsilon)$ of the scalar field in the given background perturbs the spacetime at the second order $\mathcal{O}(\epsilon^2)$ [39], i.e., to leading order, we can treat this scalar perturbation as a probe into the background with a fixed geometry. Therefore the following perturbation equation is

$$D_\mu D^\mu \Phi = 0, \tag{9}$$

where $D_\mu \equiv \nabla_\mu - ieA_\mu$, A_μ is the electromagnetic potential four-vector above, and e the test charge of the scalar field.

The source-free Maxwell field $\mathcal{F}_{ab}$ has been imposed in [15] and the vector-potential is given by

$$A = -\frac{Q}{r}dt. \tag{10}$$

The equation of motion (9) can be separated into

$$\Phi(t, r, \theta, \varphi) = \sum_{lm} \int d\omega\, e^{-i\omega t} \frac{\phi(r)}{r} Y_{lm}(\theta, \varphi), \tag{11}$$

where $Y_{lm}(\theta, \varphi)$ is the spherical harmonics for the 2-sphere S^2. Hence (9) remains the radial equation

$$\begin{aligned}&\phi(r)[(eQ - r\omega)^2 - rf(r)(l(l+1)r + f'(r))] \\ &\quad + r^2 f(r) f'(r)\phi'(r) + r^2 f^2(r)\phi'(r) = 0.\end{aligned} \tag{12}$$

The main difference between this equation and the uncharged case is the introduction of $(eQ - r\omega)^2$ term, which brings the first power term of ω and modifies the boundary behavior at the horizon.

III. THE METHODS

In this section we summarize the three methods we will use in our computation of quasinormal modes.

A. The WKB method

For WKB method, Eq. (12) is conventionally reduced to the Schrödinger-like equation by taking the tortoise coordinate $dr_* = dr/f(r)$,

$$\frac{d^2\phi(r)}{dr_*^2} = [V(\omega, r) - \omega^2]\phi(r), \tag{13}$$

$$V(\omega, r) = \frac{2eQ\omega}{r} + \frac{e^2Q^2}{r^2} - l(l+1)f(r) - \frac{f(r)f'(r)}{r}, \tag{14}$$

where r_* ranges from $-\infty$ at the horizon to $+\infty$ at the radial infinity. This Schrödinger-like equation has an effective potential barrier (Fig. 1) between the horizon and the radial infinity for both first and second kind aether black hole, where the ω-dependence is assumed to be $\omega = 1$. These effective potentials depend on the frequency ω for charged scalar perturbation, which is different from the uncharged case [19,40,41]. However the WKB method is also suitable for this effective potential [40,42,43] when the quasinormal modes satisfy the condition $\mathrm{Re}(\omega) > 0$ [43]. The scheme to solve this problem will be discussed in detail below.

The WKB method can semianalytically calculate the quasinormal modes which satisfy the suitable boundary conditions (ingoing for horizon and outgoing for spatial infinity). The first-order WKB was first used by Schutz and Will [44], and the third-order WKB was given by Iyer and Will [40] two years later. After that this method was extended to the sixth-order by Konoplya [42] and to the thirteenth-order by Matyjasek and Opala [45]. The higher-order WKB formula is given by [43]

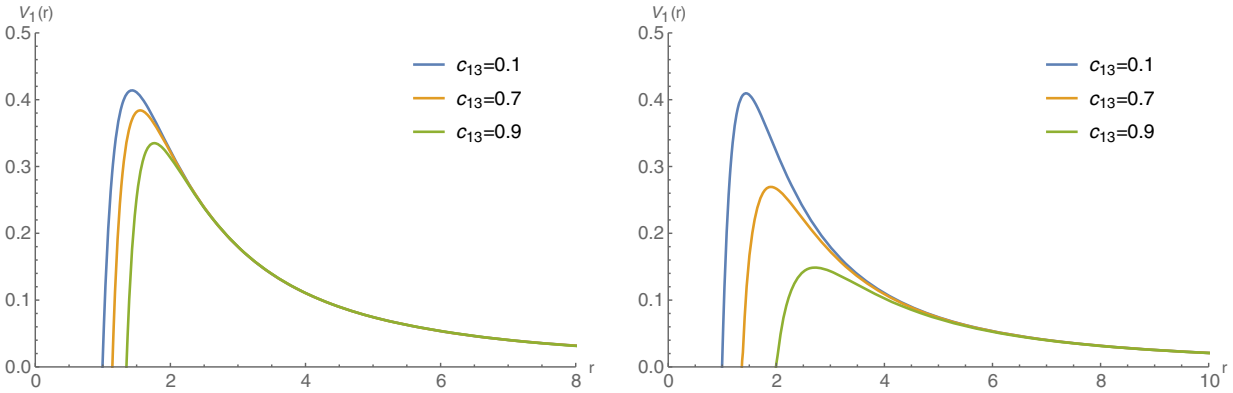

FIG. 1. The effective potential for the first kind aether black hole (left) and the second kind aether black hole (right) with $l = 1, e = 0.1, Q = 0.1, r_0 = 1$.

$$0 = U_0(\omega) + A_2(\mathcal{K}^2) + A_4(\mathcal{K}^2) + A_6(\mathcal{K}^2) + \ldots - i\mathcal{K}\sqrt{-2U_2(\omega)}(1 + A_3(\mathcal{K}^2) + A_5(\mathcal{K}^2) + A_7(\mathcal{K}^2) + \ldots), \tag{15}$$

where

$$\mathcal{K} = n + \frac{1}{2}, \quad U_0(\omega) = U(\omega, r_{\max}),$$
$$U_2(\omega) = \frac{d^2U(\omega,r)}{dr_*^2}\bigg|_{r=r_{\max}}, \quad U_3(\omega) = \frac{d^3U(\omega,r)}{dr_*^3}\bigg|_{r=r_{\max}}, \ldots. \tag{16}$$

The $r_{\max}$ denotes the value of coordinate r where the effective potential (14) reaches its maximum and the n is the overtone number. The $A_i(\mathcal{K}^2)$ is the correction of order i which depends on $\mathcal{K}^2$ and the values $U_2, U_3, \ldots$ of higher derivatives of U_0. For charged scalar perturbation, the $U(\omega, r)$ can be expended by $V(\omega, r) - \omega^2$. Hence the WKB formula becomes

$$\omega^2 = V_0(\omega) + A_2(\mathcal{K}^2) + A_4(\mathcal{K}^2) + A_6(\mathcal{K}^2) + \ldots - i\mathcal{K}\sqrt{-2V_2(\omega)}(1 + A_3(\mathcal{K}^2) + A_5(\mathcal{K}^2) + A_7(\mathcal{K}^2) + \ldots), \tag{17}$$

where the meanings of $V_0, V_2, \ldots$ are similar to $U_0, U_2, \ldots$ above.

The accuracy of third-order WKB has been verified for the low-lying modes $n < l$ [41,46] and has significant error for $n > l$. However the result cannot be improved by simply increasing the WKB formula order due to the asymptotical convergence of the WKB method [47]. The Padé approximants can be used to improve the accuracy of the higher-order WKB method [43]. This approach starts by defining a polynomial $P_k(\epsilon)$

$$P_k(\epsilon) = V_0(\omega) + A_2(\mathcal{K}^2)\epsilon^2 + A_4(\mathcal{K}^2)\epsilon^4 + A_6(\mathcal{K}^2)\epsilon^6 + \ldots - i\mathcal{K}\sqrt{-2V_2(\omega)}(\epsilon + A_3(\mathcal{K}^2)\epsilon^3 + A_5(\mathcal{K}^2)\epsilon^5 + \ldots), \tag{18}$$

and it returns to WKB formula (17) by taking $\epsilon = 1$,

$$\omega^2 = P_k(1). \tag{19}$$

Next we can construct a family of rational functions called Padé approximants

$$P_{\tilde{n}/\tilde{m}}(\epsilon) = \frac{Q_0 + Q_1\epsilon + \cdots + Q_{\tilde{n}}\epsilon^{\tilde{n}}}{R_0 + R_1\epsilon + \cdots + R_{\tilde{m}}\epsilon^{\tilde{m}}} \tag{20}$$

with $\tilde{n} + \tilde{m} = k$. The divergence between Padé approximants and pure WKB formula is given by $O(\epsilon^{k+1})$ near $\epsilon = 0$.

However the turning point $r_{\max}$ cannot be evaluated directly due to the ω-dependence of the effective potential $V(\omega, r)$ and the correction $A_i(\mathcal{K}^2)$ will become a rather complicated function of ω with increasing of i. In more detail, Matyjasek and Opala [45] showed the number of terms in A_i, where the A_6 has 294 terms and the A_{13} has even 22050 terms. Moreover, the Padé approximants further increase the computational complexity.

If we treat ω as real-value, the turning point $r_{\max}$ of effective potential becomes a numerical function of ω when fixes all the other parameters [48]. The following procedure is given by Konoplya [42]: substituting the numerical function into Eq. (17) and the quasinormal frequency is obtained by finding the root of this equation. More specifically, we move ω^2 to the right of Eq. (17) and regard the right part as a numerical complex function on the complex ω plane. For a given ω, the $r_{\max}$ can be found and then the value of the numerical complex function is obtained through the open *Mathematica* package [49]. Through an iterative program, the quasinormal frequency is determined by the approximation of the function value to zero.

In this paper, we use sixth-order WKB formula with padé approximants $P_{5/1}(1)$ to reproduce the results in [8] and calculate the charged case.

B. The continued fraction method

Since Leaver first reported the results of quasinormal modes calculated by the continued fraction method [50], this method has been widely used in the study of scalar perturbations under different black hole theories. However, it is difficult to obtain a complete three-term recurrence formula including all theoretical parameters. We use the numerical program to obtain the three-term recurrence formula, which will be expanded in detail below.

Equation (12) can be written in a different form

$$f(r)\left(p(r)\frac{d^2}{dr^2} + \frac{d}{dr} + q(r,\omega)\right)\phi(r) = 0. \tag{21}$$

When we fix all the parameters $(e, Q, c_{13}, c_{14}, r_0, l)$, the Frobenius series can be constructed as [3]

$$e^{-I(\omega)r}r^{-I(\omega)}\left(\frac{r - r_h}{r}\right)^{H(\omega)}\sum_{k=0}^{\infty} b_k\left(\frac{r - r_h}{r}\right)^k, \tag{22}$$

where $I(\omega)$, $H(\omega)$ are functions of purely ω and defined by the boundary conditions of Eq. (21). For instance, both $I(\omega)$ and $H(\omega)$ are $-i\omega$ for massless scalar perturbation of Schwarzschild black hole.

The Frobenius Series (22) can be truncated to N and substituted into (21). The N-term recurrence relation for the coefficients b_k is

$$\sum_{j=0}^{\min(N-1,i)} c_{j,i}^{(N)} b_{i-j} = 0, \quad \text{for } i > 0. \tag{23}$$

Then, the Gaussian eliminations allows one to reduce the N-term recurrence relation to the three-term recurrence relation [3]

$$c_{0,i}^{3} b_i + c_{1,i}^{(3)} b_{i-1} + c_{2,i}^{(3)} b_{i-2} = 0, \quad \text{for } i > 1,$$
$$c_{0,1}^{(3)} b_1 + c_{1,1}^{(3)} b_0 = 0. \tag{24}$$

In our cases, the derivations of the three-term recurrence relations can be executed from Eq. (23) by the *Mathematica* program step by step. Here, we can find b_1/b_0 from the recurrence relation (24) in two ways:

$$\frac{b_1}{b_0} = -\frac{c_{1,1}^{(3)}}{c_{0,1}^{(3)}} = -\cfrac{c_{2,2}^{(3)}}{c_{1,2}^{(3)} - \cfrac{c_{0,2}^{(3)} c_{2,3}^{(3)}}{c_{1,3}^{(3)} - \cfrac{c_{0,3}^{(3)} c_{2,4}^{(3)}}{c_{1,4}^{(3)} - \cdots}}}. \tag{25}$$

And the final equation with respect to the coefficients of the three-term recurrence relations is given by

$$c_{1,1}^{(3)} - \cfrac{c_{0,1}^{(3)} c_{2,2}^{(3)}}{c_{1,2}^{(3)} - \cfrac{c_{0,2}^{(3)} c_{2,3}^{(3)}}{c_{1,3}^{(3)} - \cdots}} = 0. \tag{26}$$

Recall that Eq. (26) holds only if ω is the quasinormal frequency. We choose this equation as the basis for judging whether ω is the quasinormal frequency. The procedure is the following: determining the value of ω and substituting it into Eq. (22); then the coefficients $c_{j,i}^{(N)}$ of Eq. (23) become complex numbers, which can be conveniently reduced to the three-term recurrence relation (24) by the program; the coefficient of the three-term recurrence relation can be used to construct the left part of Eq. (26), that is, finally we obtain the result as a complex number, which represents the left part of Eq. (26). If this complex number is zero, we can conclude that the ω is the quasinormal frequency. Therefore we turn the problem into searching the zero point of the complex function [the left part of Eq. (26)] numerically on the complex ω plane.

C. The generalized eigenvalue method

This numerical method developed by Jansen [51] is finding the quasinormal modes by discretizing the perturbation equation and solving the resulting generalized eigenvalue equation. This method is convenient to work under the ingoing Eddington-Finkelstein coordinate

$$ds^2 = -f(z)dv^2 - 2z^{-2}dvdz + z^{-2}d\Omega_2^2, \tag{27}$$

where $z \equiv 1/r$ and $v \equiv t + r_*$. Substituting it into (9) and separating the result equation by

$$\Phi(v, z, \theta, \varphi) = \sum_{lm} \int d\omega\, e^{-i\omega v} \phi(z) Y_{lm}(\theta, \varphi). \tag{28}$$

The remain radial equation is

$$(lz + l^2 z - ieQz + 2i\omega)\phi(z) + (2iz(eQz - \omega) - z^3 f'(z))\phi'(z) - z^3 f(z)\phi''(z) = 0. \tag{29}$$

Then we need to apply appropriate boundary behaviors to satisfy the ingoing boundary condition near the horizon and the outgoing boundary condition near the infinity. The main idea of this operation is rescaling the equation to make the inappropriate solution (the non-normalizable solution or the solution which does not satisfy the boundary conditions) pathological, diverging, and rapidly oscillating. According to this idea, we redefine

$$\phi(z) \to e^{2\omega i/z} z^{-2\omega i} \phi(z), \tag{30}$$

and the final equation becomes

$$\left(lz + l^2 z - \frac{2\omega(-iz + 2\omega + 2z\omega)}{z} + eQ(-iz + 4\omega + 4z\omega) + \frac{2\omega(2\omega + z^2(-i + 2\omega) + z(-2i + 4\omega))f(z)}{z} + 2iz(1 + z)\omega f'(z)\right)\phi(z) + (2iz(eQz - \omega) + 4iz(1 + z)\omega f(z) - z^3 f'(z))\phi'(z) - z^3 f(z)\phi''(z) = 0. \tag{31}$$

The asymptotic behaviors of this equation near the boundary can be tested by plugging in the ansatz $\phi(z) = (1/r_h - z)^p$ at the horizon and $e^{p/z} z^{1-p}$ at the spatial infinity. There are only ingoing waves to the horizon and outgoing waves to the infinity, while the ingoing modes from infinity diverge.

Next we choose the Chebyshev grid to discretize this equation and the n-order derivative is replacing by the $N \times N$ matrix $D_{ij}^{(n)}$ [51]. The result matrix equation of (31) depends on the square of frequency ω

$$(\tilde{M}_0 + \omega \tilde{M}_1 + \omega^2 \tilde{M}_2)\phi = 0. \tag{32}$$

The generalized eigenvalue equation only requires first power of frequency, so we can define

$$M_0 = \begin{pmatrix} \tilde{M}_0 & \tilde{M}_1 \\ 0 & \mathbb{1} \end{pmatrix}, \qquad M_1 = \begin{pmatrix} 0 & \tilde{M}_2 \\ -\mathbb{1} & 0 \end{pmatrix}, \tag{33}$$

where 1 is the N-dimensional identity matrix. These $2N \times 2N$ matrices above act on the vector $\Phi \equiv (\phi, \omega\phi)$ and the resulting equation is

$$(M_0 + \omega M_1)\Phi = 0. \tag{34}$$

The more details are presented by Jansen in [51].

IV. QUASINORMAL MODES

In this section, we investigated the fundamental quasinormal mode ($n = 0$) for the charged scalar perturbation in the background of the Einstein-Maxwell-aether black hole. We focus on the lower multipole numbers ($l = 0, 1, 2$) and set $r_0 = 1$ by convention, which implies that the dimensionaless frequency should be taken as $\omega \to 2\omega$ [41].

For the results, we define a relative effect between the results of aether cases and non-aether cases (Schwarzschild black hole for uncharged scalar perturbation and RN black hole for charged scalar perturbation) of continued fraction method as

$$\delta_{\mathrm{Re}} = \frac{|\mathrm{Re}\,\omega_i - \mathrm{Re}\,\omega_0|}{\mathrm{Re}\,\omega_0} \times 100\% \tag{35}$$

$$\delta_{\mathrm{Im}} = \frac{|\mathrm{Im}\,\omega_i - \mathrm{Im}\,\omega_0|}{\mathrm{Im}\,\omega_0} \times 100\%, \tag{36}$$

where ω_i is the result of different c_{13} and ω_0 is the mode without aether field.

A. Spectrum of uncharged black hole

First we analyze the accuracy of the continued fraction method and the generalized eigenvalue method by comparing the results among these methods. In Tables I and II, we show the results obtained by Churilova [8] through the sixth-order WKB formula at the first line, the continued fraction method at the second line and the generalized eigenvalue method at the third line. We calculate the extra values for $l = 1$ to make a better comparison. For the aether cases, the results of these methods turn out to be in good agreement with each other for the different values of c_{13}, especially for the continued fraction method and the generalized eigenvalue method.

TABLE I. Fundamental modes of the uncharged cases for the first kind aether black hole with $Q = 0$, $e = 0$, obtained by WKB (first line), continued fraction method (second line) and generalized eigenvalue method (third line).

	$\ell = 0$			$\ell = 1$		
Parameter	QNM	Effect %		QNM	Effect %	
c_{13}	ω	δ_{Re}	δ_{Im}	ω	δ_{Re}	δ_{Im}
	$0.110678 - 0.104424i$			$0.292932 - 0.097660i$		
0	$0.110455 - 0.104896i$	0	0	$0.292936 - 0.097660i$	0	0
	$0.110455 - 0.104896i$			$0.292936 - 0.097660i$		
	$0.109637 - 0.105590i$			$0.291163 - 0.098740i$		
0.15	$0.109300 - 0.106164i$	0.99	1.2	$0.291167 - 0.098754i$	0.6	1.1
	$0.109300 - 0.106164i$			$0.291167 - 0.098754i$		
	$0.107641 - 0.105651i$			$0.288751 - 0.100052i$		
0.3	$0.107708 - 0.107620i$	2.5	2.6	$0.288760 - 0.100062i$	1.4	2.5
	$0.107708 - 0.107620i$			$0.288760 - 0.100062i$		
	$0.104550 - 0.107923i$			$0.285297 - 0.101644i$		
0.45	$0.105418 - 0.109303i$	4.5	4.2	$0.285311 - 0.101651i$	2.6	4.1
	$0.105418 - 0.109302i$			$0.285311 - 0.101651i$		
	$0.101186 - 0.110012i$			$0.279946 - 0.103602i$		
0.6	$0.101901 - 0.111241i$	7.8	6.0	$0.279968 - 0.103611i$	4.4	6.1
	$0.101901 - 0.111240i$			$0.279968 - 0.103611i$		
	$0.095375 - 0.112333i$			$0.270482 - 0.105977i$		
0.75	$0.095816 - 0.113345i$	13	8.1	$0.270476 - 0.106006i$	7.7	8.5
	$0.095816 - 0.113345i$			$0.270476 - 0.106006i$		
	$0.082006 - 0.114565i$			$0.247339 - 0.108003i$		
0.9	$0.081840 - 0.114256i$	26	9.0	$0.247178 - 0.108068i$	16	11
	$0.081835 - 0.114258i$			$0.247179 - 0.108068i$		

TABLE II. Fundamental modes of the uncharged cases for the second kind aether black hole with $Q = 0$, $e = 0$, $c14 = 0.2$, obtained by WKB (first line), continued fractions method (second line) and generalized eigenvalue method (third line).

	$\ell = 0$			$\ell = 1$		
Parameter	QNM	Effect %		QNM	Effect %	
c_{13}	ω	δ_{Re}	δ_{Im}	ω	δ_{Re}	δ_{Im}
	$0.110678 - 0.104424i$			$0.292932 - 0.097660i$		
0.1	$0.110455 - 0.104896i$	0	0	$0.292936 - 0.097660i$	0	0
	$0.110455 - 0.104896i$			$0.292936 - 0.097660i$		
	$0.107071 - 0.103500i$			$0.283693 - 0.096589i$		
0.25	$0.106840 - 0.103974i$	3.3	0.88	$0.283699 - 0.096591i$	3.2	1.1
	$0.106840 - 0.103974i$			$0.283699 - 0.096591i$		
	$0.102441 - 0.101957i$			$0.271838 - 0.094901i$		
0.4	$0.102197 - 0.102433i$	7.5	2.3	$0.271846 - 0.094906i$	7.2	2.8
	$0.102197 - 0.102433i$			$0.271846 - 0.094906i$		
	$0.096215 - 0.099294i$			$0.255829 - 0.092123i$		
0.55	$0.095936 - 0.099779i$	13	4.9	$0.255838 - 0.092133i$	13	5.7
	$0.095936 - 0.099779i$			$0.255838 - 0.092133i$		
	$0.087179 - 0.094317i$			$0.232334 - 0.087139i$		
0.70	$0.086794 - 0.094836i$	21	9.6	$0.232341 - 0.087156i$	21	11
	$0.086794 - 0.094835i$			$0.232341 - 0.087156i$		
	$0.071753 - 0.083125i$			$0.191571 - 0.076340i$		
0.85	$0.071112 - 0.083732i$	36	20	$0.191576 - 0.076364i$	35	22
	$0.071107 - 0.083730i$			$0.191576 - 0.076364i$		

The percentages of relative effect are placed to the right of the quasinormal frequencies for each c_{13} respectively. Previously there are the relative effects obtained by third-order WKB [8]. We use more accurate results to demonstrate the aether effect on quasinormal frequencies. For the first kind aether black hole, the effects of large c_{13}, which are compared to the Schwarzschild cases, are 26 for the real part of the value and 9.0 for the imaginary part with $l = 0$. These are smaller than the effect of third-order WKB. The corresponding effects are following: 16 and 11 for the first kind aether black hole with $l = 1$, 36 and 20 for the second kind aether black hole with $l = 0$, 35 and 22 for the second kind aether black hole with $l = 1$. The relative effects for the second kind aether black hole are larger than those for the first kind, which is contrary to the results of third-order WKB for $l = 0$ presented in [8].

B. Spectrum of charged black hole

After that, We go on to the extension of the cases above, the charged scalar perturbations. The results of modes are presented in Tables III and IV for the first kind and the second kind aether black hole respectively. The results are placed one under the other as the uncharged cases. The values of the quasinormal modes for the Reissner-Nordström black hole ($c_{13} = 0$) presented in Table III are used to calculate the relative effect. Obviously, the results of the WKB method are closer to the continued fraction method than the generalized eigenvalue method. Simply increasing the resolution does not improve the accuracy of the results of the generalized eigenvalue method, resulting in a difference between it and the continued fraction method. In general, the continued fraction method provides the most accurate results compared to the other numerical methods.

The relative effects for charged scalar perturbations are similar to the uncharged case, which is, the effects for the second kind aether black hole are generally larger than the first kind. We can see that the effect of large c_{13} can even exceed 50% in Table IV.

C. Effects of charge Q on the quasinormal modes

Then We demonstrate the modes ω vs Q in Fig. 2 with fixed $r_0 = 2, e = 0.1, l = 1$ for the first kind aether black hole. The real part of the fundamental modes increases with Q monotonically. However, the imaginary part of these frequencies first decreases with Q and then increases with Q. Both the real and imaginary part of frequencies get smaller as c_{13} gets larger, which consist of Table II.

The fundamental modes of the second kind aether black hole are following. First of all, we focus on the allowable parameters range for the second kind aether black hole which is very different from the previous cases, because of the parameter constraints (8). These three parameters (Q, c_{13}, c_{14}) are intertwined, so we have to decide the parameter range according to which parameter we are varying.

TABLE III. Fundamental modes of the charged cases for the first kind aether black hole with $Q = 0.1$, $e = 0.1$, obtained by WKB (first line), continued fraction method (second line) and generalized eigenvalue method (third line).

	$\ell = 1$			$\ell = 2$		
Parameter	QNM	Effect %		QNM	Effect %	
c_{13}	ω	δ_{Re}	δ_{Im}	ω	δ_{Re}	δ_{Im}
	$0.298515 - 0.098187i$			$0.490396 - 0.097187i$		
0	$0.298408 - 0.098209i$	0	0	$0.490334 - 0.097184i$	0	0
	$0.296162 - 0.098874i$			$0.491114 - 0.096766i$		
	$0.297372 - 0.098916i$			$0.488661 - 0.097879i$		
0.1	$0.297274 - 0.098931i$	0.35	0.06	$0.488615 - 0.097866i$	0.36	0.9
	$0.295114 - 0.098816i$			$0.489344 - 0.097633i$		
	$0.296012 - 0.099719i$			$0.486593 - 0.098624i$		
0.2	$0.295894 - 0.099743i$	0.81	0.33	$0.486539 - 0.098639i$	0.77	1.9
	$0.293759 - 0.099197i$			$0.487324 - 0.098578i$		
	$0.294295 - 0.100666i$			$0.484009 - 0.099517i$		
0.3	$0.294185 - 0.100660i$	1.3	0.77	$0.483982 - 0.099520i$	1.3	3.0
	$0.292192 - 0.099639i$			$0.484797 - 0.099676i$		
	$0.292124 - 0.101662i$			$0.480820 - 0.100522i$		
0.4	$0.292015 - 0.101706i$	2.0	1.3	$0.480752 - 0.100534i$	2.0	4.3
	$0.290327 - 0.100148i$			$0.481489 - 0.100966i$		
	$0.289291 - 0.102890i$			$0.476578 - 0.101691i$		
0.5	$0.289173 - 0.102908i$	2.7	2.0	$0.476537 - 0.101712i$	1.7	5.2
	$0.288042 - 0.100862i$			$0.477082 - 0.102462i$		
	$0.285391 - 0.104261i$			$0.470854 - 0.103101i$		
0.6	$0.285288 - 0.104296i$	3.7	3.0	$0.470785 - 0.103092i$	4.1	7.5
	$0.285072 - 0.101867i$			$0.470848 - 0.104048i$		
	$0.279753 - 0.105835i$			$0.462483 - 0.104714i$		
0.7	$0.279630 - 0.105895i$	5.2	4.8	$0.462401 - 0.104713i$	6.0	9.1
	$0.280776 - 0.103629i$			$0.461956 - 0.105532i$		
	$0.270712 - 0.107617i$			$0.448836 - 0.106554i$		
0.8	$0.270475 - 0.107660i$	7.8	8.1	$0.448771 - 0.106560i$	8.8	9.8
	$0.273199 - 0.106902i$			$0.447697 - 0.106282i$		
	$0.252367 - 0.108843i$			$0.421103 - 0.108100i$		
0.9	$0.252062 - 0.108975i$	15	14	$0.421016 - 0.108109i$	14	11
	$0.252412 - 0.112625i$			$0.421709 - 0.107267i$		

First we demonstrate the fundamental modes with different Q and Fig. 3 shows the allowable range of Q obtained by constraints (8), where different curves denote the different choice of c_{13}. This plot reveals that the allowable range of Q decreases with c_{14} and even goes to zero as c_{14} goes to its extreme values. In order to show more behaviors of the quasinormal modes, we always choose the value of fixed parameters c_{14} which can lead to a larger parameter range of the varying parameter Q. In this case, small c_{14} generates a large range of Q, so we fix $c_{14} = 0.1$ and the results are shown by Fig. 4. These plots show that the real part ω_R increases with Q and the imaginary part ω_I decreases with Q. The larger c_{13} leads to smaller ω_R and larger ω_I.

We next show the parameters allowable range in Fig. 5 and the fundamental modes with different c_{14} in Fig. 6. The parametric constraints derived from the constraints (8) are given by

$$\frac{4Q^2}{r_0^2} < c_{13} < 1, \qquad 0 < c_{14} \leq \frac{-8Q^2 + 2c_{13}r_0^2}{r_0^2}. \tag{37}$$

In the same way, we choose the left plot ($c_{13} \to c_{13\ \max}$) because of the larger allowable range of c_{14}. In Fig. 6, the real part of frequencies increases with c_{14} monotonically and the imaginary part of frequencies decreases with c_{14} monotonically.

It should be noted that the modes with different fixed parameters tend to be consistent while the variable parameters tend to be the maximum value both in Fig. 4 and 6. The reason for this similar behavior is that the metric function (7) becomes the Schwarzschild case while the variable parameters take the maximum value.

TABLE IV. Fundamental modes of the charged cases for the second kind aether black hole with $Q = 0.1$, $e = 0.1$, $c14 = 0.2$, obtained by WKB (first line), continued fractions method (second line) and generalized eigenvalue method (third line).

	$\ell = 1$			$\ell = 2$		
Parameter	QNM	Effect %		QNM	Effect %	
c_{13}	ω	δ_{Re}	δ_{Im}	ω	δ_{Re}	δ_{Im}
	$0.295850 - 0.097916i$			$0.486082 - 0.096894i$		
0.15	$0.295782 - 0.097947i$	0.8	1.2	$0.486059 - 0.096914i$	0.88	0.02
	$0.293726 - 0.097687i$			$0.486787 - 0.096749i$		
	$0.289457 - 0.097198i$			$0.475662 - 0.096160i$		
0.25	$0.289374 - 0.097230i$	2.8	2.9	$0.475623 - 0.096180i$	3.0	0.26
	$0.287875 - 0.095979i$			$0.476295 - 0.096520i$		
	$0.281878 - 0.096256i$			$0.463344 - 0.095184i$		
0.35	$0.281804 - 0.096249i$	5.0	4.5	$0.463294 - 0.095183i$	5.6	0.88
	$0.281364 - 0.094458i$			$0.463508 - 0.095919i$		
	$0.272759 - 0.094857i$			$0.448459 - 0.093790i$		
0.45	$0.272674 - 0.094888i$	7.6	5.6	$0.448418 - 0.093807i$	8.8	2.5
	$0.273514 - 0.093325i$			$0.447911 - 0.094392i$		
	$0.261437 - 0.092922i$			$0.430002 - 0.091843i$		
0.55	$0.261352 - 0.092950i$	11	6.3	$0.429962 - 0.091855i$	13	5.3
	$0.263099 - 0.092647i$			$0.429258 - 0.091596i$		
	$0.246798 - 0.090055i$			$0.406182 - 0.088968i$		
0.65	$0.246753 - 0.090077i$	16	7.3	$0.406144 - 0.088974i$	17	8.8
	$0.247651 - 0.091666i$			$0.406323 - 0.088281i$		
	$0.226836 - 0.085443i$			$0.373518 - 0.084436i$		
0.75	$0.226766 - 0.085531i$	24	13	$0.373498 - 0.084431i$	24	12
	$0.225215 - 0.086017i$			$0.374071 - 0.084820i$		
	$0.196390 - 0.077350i$			$0.323737 - 0.076333i$		
0.85	$0.196333 - 0.077411i$	33	23	$0.323698 - 0.076348i$	34	21
	$0.197072 - 0.076325i$			$0.323221 - 0.076001i$		
	$0.135844 - 0.057626i$			$0.224452 - 0.056835i$		
0.95	$0.135865 - 0.057691i$	54	42	$0.224429 - 0.056803i$	54	41
	$0.135386 - 0.057071i$			$0.224014 - 0.056833i$		

V. QUASIRESONANCE

In this section we study the massive charged scalar perturbation. The general covariant equation of a massive charged scalar field is given by

$$(D_\mu D^\mu - \mu^2)\Phi = 0. \tag{38}$$

There is so-called quasiresonance, which is the arbitrarily long-living mode when the field mass approaches some special values. The quasiresonance can also be considered as the bound-state problem at the zero damping rate limit [21]. The imaginary part of frequency $\mathrm{Im}(\omega)$ increases with the increasing of the field mass μ. When $\mathrm{Im}(\omega)$ approaches zero, the amplitude of field function vanishes both at the

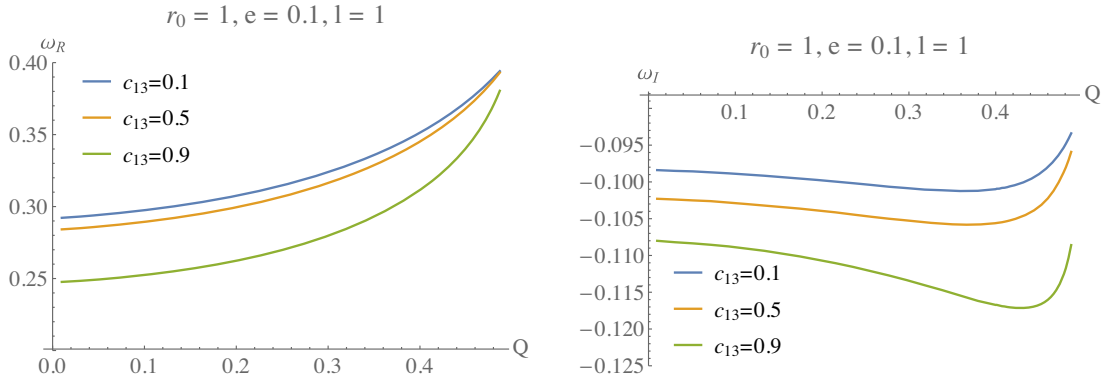

FIG. 2. The fundamental modes of charged scalar perturbation vs Q at $r_0 = 1, e = 0.1, l = 1$ for the first kind aether black hole.

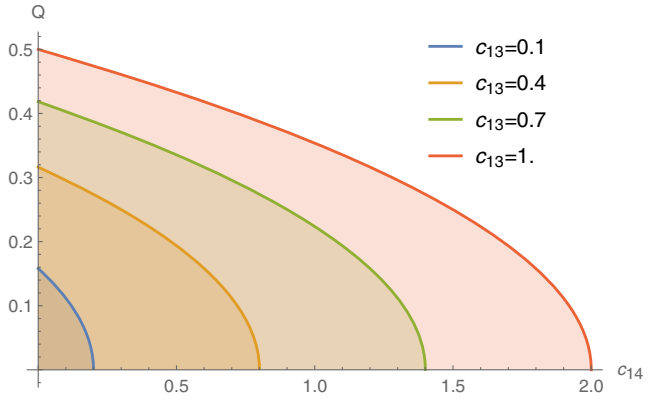

FIG. 3. The allowable range of Q for the second kind aether black hole.

horizon and infinity because of the energy conservation. Konoplya found that the existence of quasiresonance is due to the nonzero value of potential energy at spatial infinity [22].

In [8], Churilova shows that the WKB method cannot be fully trusted for the calculation of quasiresonance. Hence we choose the continued fraction method to calculate the quasiresonance. To do this, We need to take into consideration the subdominant asymptotic term at infinity:

$$\phi(r) \sim e^{-I(\omega)r} r^{\mu^2/2I(\omega)}, \qquad r \to +\infty, \tag{39}$$

where $\phi(r)$ is the radial part of Φ after separating variables. The following appropriate series is given by

$$\phi(r) = e^{-I(\omega)r}\, r^{-I(\omega)+\mu^2/2I(\omega)} \left(\frac{r-r_h}{r}\right)^{H(\omega)} \sum_{k=0}^{\infty} b_k \left(\frac{r-r_h}{r}\right)^k. \tag{40}$$

Figures 7–9 demonstrate that increasing of the field mass μ decreases $-\mathrm{Im}(\omega)$ up to zero. We confirmed that the quasiresonances exist for the case of the massive charged scalar field in the Einstein-Maxwell-aether black hole spacetime even with large c_{13}. Comparing Fig. 9 with Figs. 7 and 8, we find that the large c_{13} decreases the critical field mass μ where $\mathrm{Im}(\omega)$ approaches zero.

VI. DISCUSSION

In this paper, we studied the fundamental modes of the charged scalar perturbations in the background of two kinds of Einstein-Maxwell-aether black holes. These detailed modes with different system parameter(c_{13}, Q, c_{14}) are demonstrated by tables and figures. There are three methods, the WKB method with Padé approximants, continued fraction method and generalized eigenvalue method used in the calculations. We proposed a new numerical program for the continued fraction method and verified its effectiveness

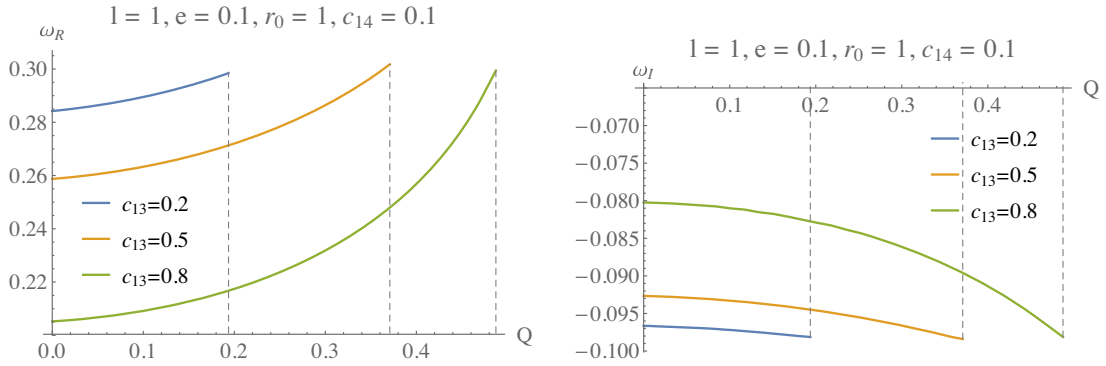

FIG. 4. The left and the right plot are ω_{R} and ω_{I} of the fundamental modes vs Q at $l = 1, e = 0.1, r_0 = 2, c_{14} = 0.1$.

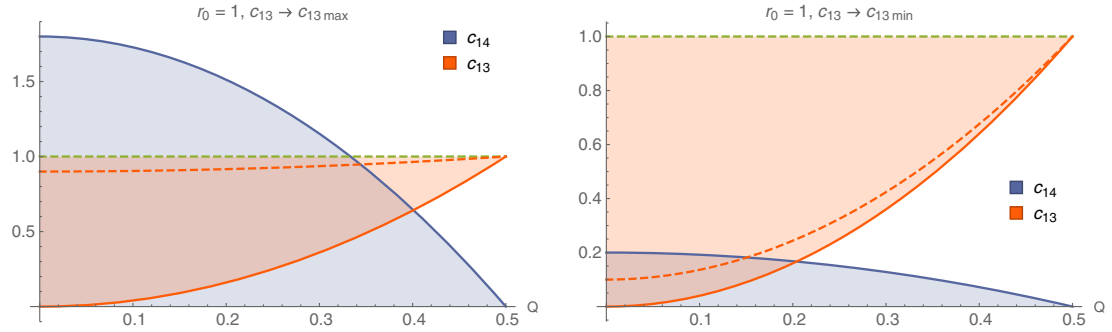

FIG. 5. The allowable range of c_{13} (red) and c_{14} (blue) for the second kind aether black hole with different Q. The red dashed line denotes the actual value of c_{13} which can change the size of the allowable range of c_{14}.

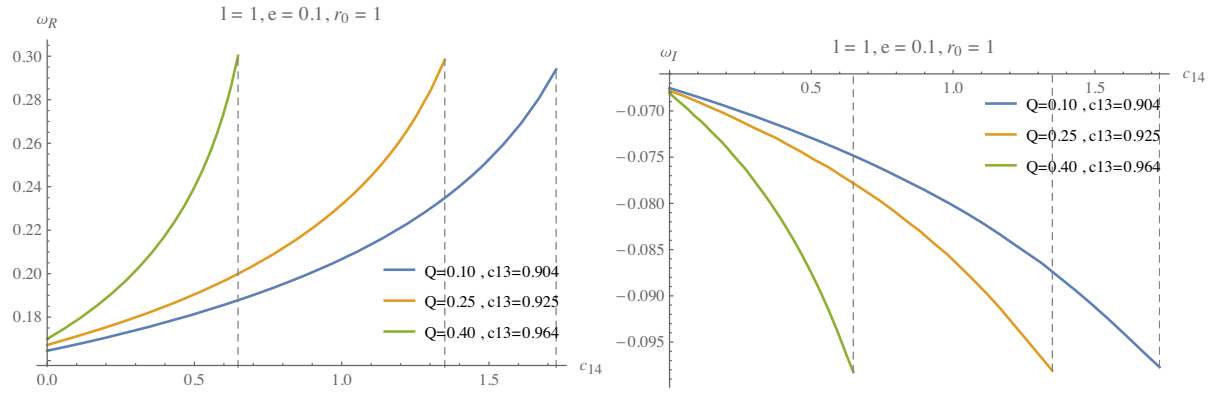

FIG. 6. The left and the right plot are ω_{R} and ω_{I} of the fundamental modes vs c_{14} at $l = 1, e = 0.1, r_0 = 2, c_{13} \to c_{13\,\max}$.

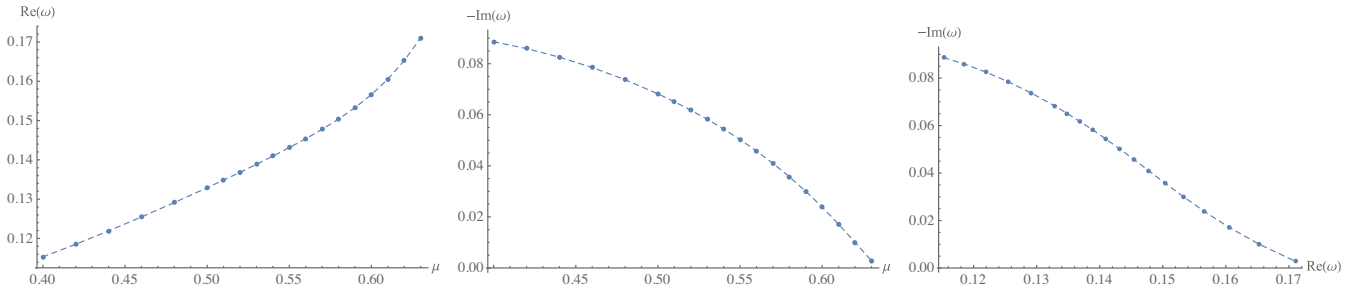

FIG. 7. The fundamental modes, calculated by the continued fraction method, for the first kind aether black hole ($e = 0.1, Q = 0.1, r_0 = 1, c_{13} = 0.5, l = 0$): real parts vs μ (left panel); imaginary parts vs μ (middle panel); imaginary parts vs real parts (right panel).

by comparing the results of different methods. In general, the continued fraction method provides the most accurate results of quasinormal modes. The effect of the aether parameter c_{14} has not been investigated in previous studies, which is included in our content. We analyzed the allowed region obtained by the constraints of parameter for the second kind aether black hole. Finally we calculated the spectrum of the massive perturbations and confirmed the quasiresonances in the Einstein-Maxwell-aether theory.

There are several topics worthy of further study. In recent years, the detections of GW by the Advanced LIGO and Advanced Virgo detectors allow us to put constraints on the modified gravity theory. The dimensionless coupled constants c_i in the Einstein-aether model have been stringently restricted by the range of derivation of the speed of GW from the speed of light [52,53]. Even the future detections of gravitational slip would validate the vector-tensor theories that contain the Einstein-aether theory [54]. Furthermore, the study of the quasinormal mode spectrum in the Einstein-aether model can also place observational constraints on the c_i and provide the sensitive test of general relativity. However, the current observation signals of ringdown only include gravitational radiation and the radiation of the matter field is absent [55]. On the other

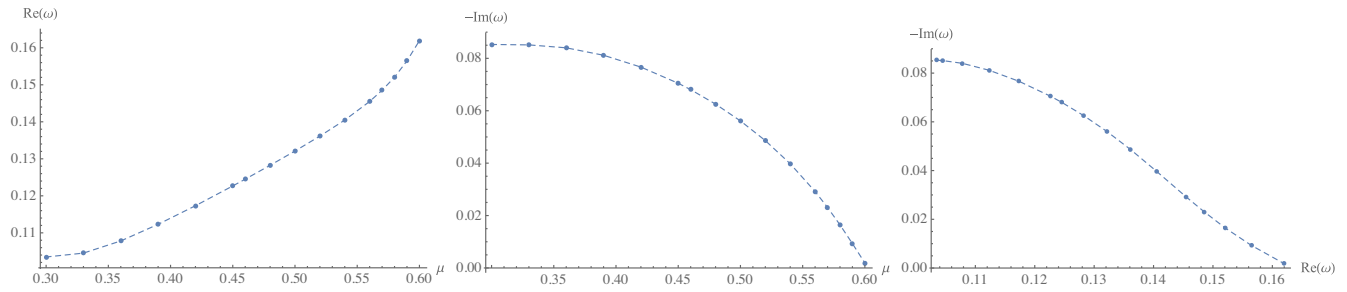

FIG. 8. The fundamental modes, calculated by the continued fraction method, for the second kind aether black hole ($e = 0.1, Q = 0.1, r_0 = 1, c_{13} = 0.45, c_{14} = 0.2, l = 0$): real part vs μ (left panel); imaginary part vs μ (middle panel); imaginary part vs real part (right panel).

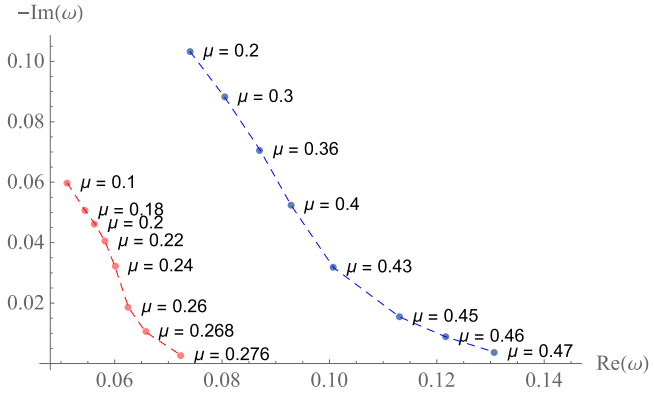

FIG. 9. Dependence of the imaginary part of the fundamental mode ($e = 0.1, Q = 0.1, r_0 = 1, c_{13} = 0.95, l = 0$) for the first kind (blue line) and the second kind (red line) aether black hole with $c_{14} = 0.2$.

hand, we must also take into account the rotating aether black holes, because current observed data demonstrate that postmerger black holes have nonzero spin. The numerical stationary solutions of rotating aether black holes have been investigated in [56]. Therefore, to present the credible constraint on Einstein-Maxwell-aether theory by quasinormal modes, one must perform the calculation of metric perturbations on the background of rotating aether black holes. As Churilova points out that the full set of perturbation equations including the energy-momentum tensor of the aether field and the Maxwell field are necessary for the reliable result of the gravitational perturbation in the Einstein-Maxwell-aether theory [8]. This will be significant but challenging.

As an attempt, we use the error bar ($\delta\hat{f}_{220} = 0.02^{+0.07}_{-0.07}$, $\delta\hat{\tau}_{220} = 0.13^{+0.21}_{-0.22}$) of QNMs in [55] and regard it as the potential relative effects of aether, where $\hat{f}_{220}$ and $\hat{\tau}_{220}$ are the frequency and the damping time of the (2,2,0) QNM of gravitational waves. The preliminary dimensionless parameter constraint on the first kind aether black hole is $c_{13} < 0.4753$ by comparing the results of scalar perturbation with $Q = 0, e = 0, l = 0$. Of course, it is not rigorous, but it has certain reference value.

The charged scalar perturbation of the Einstein-Maxwell-aether black holes coupled with the cosmological constant is also an open question. These black hole solutions have been presented by Ding in [15]. The effect of aether on the so-called superradiant instability in that situation is worth investigating.

ACKNOWLEDGMENTS

Peng Liu would like to thank Yun-Ha Zha for her kind encouragement during this work. This work is supported by the Natural Science Foundation of China under Grants No. 11805083, No. 11905083, No. 12005077 and Guangdong Basic and Applied Basic Research Foundation (2021A1515012374).

[1] E. Berti, V. Cardoso, and A. O. Starinets, Quasinormal modes of black holes and black branes, Classical Quantum Gravity **26**, 163001 (2009).
[2] K. D. Kokkotas and B. G. Schmidt, Quasinormal modes of stars and black holes. Living Rev. Relativity **2**, 2 (1999).
[3] R. A. Konoplya and A. Zhidenko, Quasinormal modes of black holes: From astrophysics to string theory, Rev. Mod. Phys. **83**, 793 (2011).
[4] S. Chandrasekhar, *The Mathematical Theory of Black Holes*, 3rd ed. (Clarendon Press, Oxford, 1985).
[5] D. S. Eniceicu and M. Reece, Quasinormal modes of charged fields in Reissner–Nordstrom backgrounds by Borel–Padé summation of Bender–Wu series, Phys. Rev. D **102**, 044015 (2020).
[6] B. P. Abbott *et al.* (LIGO Scientific and Virgo Collaborations), Observation of Gravitational Waves from a Binary Black Hole Merger, Phys. Rev. Lett. **116**, 061102 (2016).
[7] B. P. Abbott *et al.* (LIGO Scientific and Virgo Collaborations), Tests of General Relativity with GW150914, Phys. Rev. Lett. **116**, 221101 (2016).
[8] M. S. Churilova, Black holes in Einstein-aether theory: Quasinormal modes and time-domain evolution, Phys. Rev. D **102**, 024076 (2020).
[9] D. Mattingly, Modern tests of lorentz invariance, Living Rev. Relativity **8**, 5 (2005).
[10] M. R. Douglas and N. A. Nekrasov, Noncommutative field theory, Rev. Mod. Phys. **73**, 977 (2001).
[11] T. Zhu, Q. Wu, M. Jamil, and K. Jusufi, Shadows and deflection angle of charged and slowly rotating black holes in Einstein-Æther theory, Phys. Rev. D **100**, 044055 (2019).
[12] C. Ding, A. Z. Wang, X. W. Wang, and T. Zhu, Hawking radiation of charged Einstein-aether black holes at both Killing and universal horizons, Nucl. Phys. **B913**, 694 (2016).
[13] K. Lin, V. H. Satheeshkumar, and A. Z. Zhong, Static and rotating universal horizons and black holes in gravitational theories with broken Lorentz invariance, Phys. Rev. D **93**, 124025 (2016).
[14] T. Jacobson and D. Mattingly, Generally covariant model of a scalar field with high frequency dispersion and the cosmological horizon problem, Phys. Rev. D **63**, 041502 (2001).
[15] C. Ding, A. Wang, and X. Wang, Charged Einstein-aether black holes and Smarr formula, Phys. Rev. D **92**, 084055 (2015).
[16] R. Ghosh, Akash. K. Mishra, and S. Sarkar, Overcharging extremal black holes, Phys. Rev. D **104**, 104043 (2021).

[17] J. Bhattacharyya and D. Mattingly, Universal horizons in maximally symmetric spaces, Int. J. Mod Phys. D **13**, 1443005 (2014).
[18] R. A. Konoplya and A. Zhidenko, Gravitational spectrum of black holes in the Einstein–Aether theory, Phys. Lett. B **648**, 236 (2007).
[19] C. Ding, Gravitational quasinormal modes of black holes in Einstein-aether theory, Nucl. Phys. **B938**, 736 (2019).
[20] C. Ding, Quasinormal ringing of black holes in Einstein-aether theory, Phys. Rev. D **96**, 104021 (2017).
[21] R. A. Konoplya and A. Zhidenko, A massive charged scalar field in the Kerr-Newman background I: Quasinormal modes, late-time tails and stability, Phys. Rev. D **88**, 024054 (2013).
[22] R. A. Konoplya, Decay of massive scalar field in a Schwarzschild background, arXiv:2005.0411059v2.
[23] R. A. Konoplya and A. Zhidenko, Stability and quasinormal modes of the massive scalar field around Kerr black holes, Phys. Rev. D **73**, 124040 (2006).
[24] R. A. Konoplya, Massive vector field perturbations in the Schwarzschild background: Stability and quasinormal spectrum, Phys. Rev. D **73**, 024009 (2006).
[25] C. Wu and R. Xu, Decay of massive scalar field in a black hole background immersed in magnetic field, Eur. Phys. J. C **75**, 391 (2015).
[26] A. F. Zinhailo, Quasinormal modes of the four-dimensional black hole in Einstein–Weyl gravity, Eur. Phys. J. C **78**, 992 (2018).
[27] E. Abdalla, B. Cuadros-Melgar, J. de Oliveira, A. B. Pavan, and C. E. Pellicer, Vectorial and spinorial perturbations in Galileon black holes: Quasinormal modes, quasiresonant modes, and stability, Phys. Rev. D **99**, 044023 (2019).
[28] R. A. Konoplya, A. F. Zinhailo, and Z. Stuchlík, Quasinormal modes, scattering, and Hawking radiation in the vicinity of an Einstein-dilaton-Gauss-Bonnet black hole, Phys. Rev. D **99**, 124042 (2019).
[29] A. F. Zinhailo, Quasinormal modes of Dirac field in the Einstein–Dilaton–Gauss–Bonnet and Einstein–Weyl gravities, Eur. Phys. J. C **79**, 912 (2019).
[30] R. A. Konoplya and A. Zhidenko, Quasinormal modes of massive fermions in Kerr spacetime: Long-lived modes and the fine structure, Phys. Rev. D **97**, 084034 (2018).
[31] M. S. Churilova, R. A. Konoplya, and A. Zhidenko, Arbitrarily long-lived quasinormal modes in a wormhole background, Phys. Lett. B **802**, 135207 (2020).
[32] M. S. Churilova and Z. Stuchlik, Quasinormal modes of black holes in 5D Gauss–Bonnet gravity combined with non-linear electrodynamics, Ann. Phys. (Amsterdam) **418**, 168181 (2020).
[33] C. Eling, Energy in the Einstein-aether theory, Phys. Rev. D **73**, 084026 (2006).
[34] K. Yagi, D. Blas, E. Barausse, and N. Yunes, Constraints on Einstein-aether theory and Hořava gravity from binary pulsar observations, Phys. Rev. D **89**, 084067 (2014).
[35] T. Jacobson, Einstein-aether gravity: A Status report, Proc. Sci., QG-Ph (2007) 020 [arXiv:0801.1547].
[36] T. Jacobson, Einstein-aether gravity: Theory and observational constraints, in *CPT and Lorentz Symmetry: Proceedings of the Fourth Meeting*, edited by V. A. Kostelecky (World Scientific, Singapore, Bloomington, USA, 2008), p. 92, arXiv:0711.3822.
[37] P. Berglund, J. Bhattacharyya, and D. Mattingly, Mechanics of universal horizons, Phys. Rev. D **85**, 124019 (2012).
[38] T. Jacobson and D. Mattingly, Einstein-aether waves, Phys. Rev. D **70**, 024003 (2004).
[39] R. Brito, V. Cardoso, and P. Pani, Superradiance—the 2020 Edition, Lect. Notes Phys. **906**, 1 (2015).
[40] S. Iyer and C. M. Will, Black-hole normal modes: A WKB approach. I. Foundations and application of a higher-order WKB analysis ofpotential-barrier scattering, Phys. Rev. D **35**, 3621 (1987).
[41] S. Iyer, Black-hole normal modes: A WKB approach. II. Schwarzschild black holes, Phys. Rev. D **35**, 3632 (1987).
[42] R. A. Konoplya, Decay of a charged scalar field around a black hole: Quasinormal modes of RN, RNAdS, and dilaton black holes, Phys. Rev. D **66**, 084007 (2002).
[43] R. A. Konoplya, A. Zhidenko, and A. F. Zinhailo, Higher order WKB formula for quasinormal modes and grey-body factors: Recipes for quick and accurate calculations, Classical Quantum Gravity **36**, 155002 (2019).
[44] B. F. Schutz and C. M. Will, Black hole normal modes - A semianalytic approach, Astrophys. J. **291**, L33 (1985).
[45] J. Matyjasek and M. Opala, Quasinormal modes of black holes: The improved semianalytic approach, Phys. Rev. D **96**, 024011 (2017).
[46] K. D. Kokkotas and B. F. Schutz, Black-hole normal modes: A WKB approach. III. The Reissner-Nordstrom black hole, Phys. Rev. D **37**, 3378 (1988).
[47] Y. Hatsuda, Quasinormal modes of black holes and Borel summation, Phys. Rev. D **101**, 024008 (2020).
[48] R. A. Konoplya, Massive charged scalar field in a Reissner-Nordstrom black hole background: Quasinormal ringing, Phys. Rev. E **101**, 042133 (2020).
[49] The *Mathematica* package with the WKB formula of 13th order and Padé approximations ready for calculation of the quasinormal modes and grey-body factors, as well as examples of such calculations for the Schwarzschild black hole are publicly available to download from [https://goo.gl/nykYGL].
[50] E. Leaver, An analytic representation for the quasi-normal modes of Kerr black holes, Proc. R. Soc. A **402**, 285 (1985).
[51] A. Jansen, Overdamped modes in Schwarzschild-de Sitter and a Mathematica package for the numerical computation of quasinormal modes, Eur. Phys. J. Plus **132**, 546 (2017).
[52] J. Oost, S. Mukohyama, and A. Wang, Constraints on Einstein-aether theory after GW170817, Phys. Rev. D **97**, 124023 (2018).
[53] T. Baker, E. Bellini, P. G. Ferreira, M. Lagos, J. Noller, and I. Sawicki, Strong Constraints on Cosmological Gravity from GW170817 and GRB 170817A, Phys. Rev. Lett. **119**, 251301 (2017).
[54] L. Amendola, M. Kunz, I. D. Saltas, and I. Sawicki, Fate of Large-Scale Structure in Modified Gravity After GW170817 and GRB170817A, Phys. Rev. Lett. **120**, 131101 (2018).
[55] R. Abbott *et al.* (LIGO Scientific, VIRGO, and KAGRA Collaborations), Tests of general relativity with GWTC-3, arXiv:2112.06861.
[56] A. Adam, P. Figueras, T. Jacobson, and T. Wiseman, Rotating black holes in Einstein-aether theory, Classical Quantum Gravity **39**, 125001 (2022).